5. Parametric study

5.1 General

This chapter incorporates the findings of the numerical modelling-based parametric study of the influence of different parameters on the volumetric strain, induced permeability trend, and seepage rate across PWBP. The major influencing parameters and their range have been obtained on the basis of the field data compiled in Table 1.1 and the permeability in Section 2.7. The changes in the distribution of induced volumetric strain and permeability in the modelled zone of interest (MZoI) formed of the nether roof, pillar, and floor, and the associated rate of water seepage has been studied for understanding the effect of these parameters on the hydro-mechanical performance of the PWBP. The thickness of the nether roof and floor was considered twice the pillar height. The baseline data of rock mass properties considered for the parametric study is given in Table 5.1. Table 5.2 summarises the range of various parameters considered in this study.

Table 5.1. Baseline data of rock mass properties

Rock layer	t, m	ρ, Kg/m^3	E, GPa	σ_c, MPa	σ_t, MPa	ϕ, °	ψ, °	ϑ	Permeability, m^2/pa.s	porosity
Roof, Floor	50	2212	8.50	11.68	1.22	40	5	0.35	4.95×10^{-10}	0.17
pillar	3	1392	2.00	3.87	0.35	25	0	0.25	2.48×10^{-11}	0.12

Where t is thickness, ρ is density, E is elastic modulus, σ_c is compressive strength, σ_c is tensile strength, ϕ is friction angle, ψ is dilation angle, ϑ is Poisson's ratio

Table 5.2 The range of various parameters

<table>
<tr><th>Sl. No.</th><th>Parameter</th><th>Range</th></tr>
<tr><td>1</td><td>Cover depth, m</td><td>100-350</td></tr>
<tr><td>2</td><td>Pillar width, m</td><td>30-120</td></tr>
<tr><td>3</td><td>Coal In-situ permeability, mD</td><td>0.5-100</td></tr>
<tr><td>4</td><td>Water head, % of cover depth</td><td>25-100</td></tr>
<tr><td>5</td><td>Rock mass strength</td><td>
<table>
<tr><th rowspan="2">Properties</th><th colspan="2">hard</th><th colspan="2">average</th><th colspan="2">soft</th></tr>
<tr><th>roof/ floor</th><th>coal</th><th>roof/ floor</th><th>coal</th><th>roof/ floor</th><th>coal</th></tr>
<tr><td>Density, kg/m^3</td><td>2373</td><td>1440</td><td>2212</td><td>1392</td><td>1879</td><td>1240</td></tr>
<tr><td>Young’s modulus, GPa</td><td>13.37</td><td>2</td><td>8.5</td><td>2</td><td>3.01</td><td>2</td></tr>
<tr><td>UCS, MPa</td><td>20.92</td><td>6.32</td><td>11.68</td><td>3.87</td><td>4.01</td><td>2.04</td></tr>
<tr><td>Tensile strength, MPa</td><td>2.39</td><td>0.71</td><td>1.22</td><td>0.35</td><td>0.39</td><td>0.04</td></tr>
</table>
</td></tr>
<tr><td>6</td><td>Flow Regimes</td><td>a. pillar only,
b. roof only,
c. floor only,
d. pillar and roof
e. pillar and floor, and
f. the pillar system (roof- pillar-floor)</td></tr>
</table>

The independent parameters included cover depth, pillar width, in-situ permeability, water head, rock mass strength, and the flow regime. The study considered possible seepage rate through the coal seam, nether floor and roof and their combinations to analyse the induced permeability and corresponding seepage rate for varying working depth, pillar width,

extraction percentage, water head, porosity, permeability, and rock-mass strength. These results were used to analyse the hydro-mechanical performance of the pillars under different geo-mining conditions. For each flow regime, the study incorporated the variation in cover depth from 100-350 m, pillar width from 15-120 m, extraction percentage from 10-44, water head from 25–100 % of cover depth, and the rock mass strength properties as given in Table 5.3.

For evaluating the influence of a parameter, its value was changed in a range while keeping the other influencing parameters to their baseline values. The baseline value was 250 m for cover depth, 125m for the water head (50% of the cover depth), and 60 m for the pillar width. The study considered a fixed pillar height of 3 m, looking into insignificant variation in the referral database compiled from the field. The zone size of 0.5 m×0.5 m was used in all the models.

The results in the following section depict flow through the pillar-only condition.

5.2 Effect of Cover Depth

The effect of depth on the volumetric strain, induced permeability distribution, and seepage rate characteristics of PWBP was studied for the cover depths of 100, 250, and 350 m. The maximum cover depth of 350 m was considered in this study based on field data compiled from the Indian geo-mining conditions.

The plots of the induced volumetric strain across a pillar width of 60 m at the cover depths of 100, 250, and 350 m (Figure 5.1) show an increase in zones of positive volumetric strain with the increase in the cover depth. The development of volumetric strain in pillars was symmetric about its central axis, irrespective of the cover depth. The failure advanced into

the pillar with the increase in cover depth, thus reducing its effective width to resist water seepage. A sharp rise in volumetric strain was observed at the edges of the pillar at cover depths of 250 and 350 m compared to 100 m. The volumetric strain at the boundaries also intensified with the increase in cover depth.

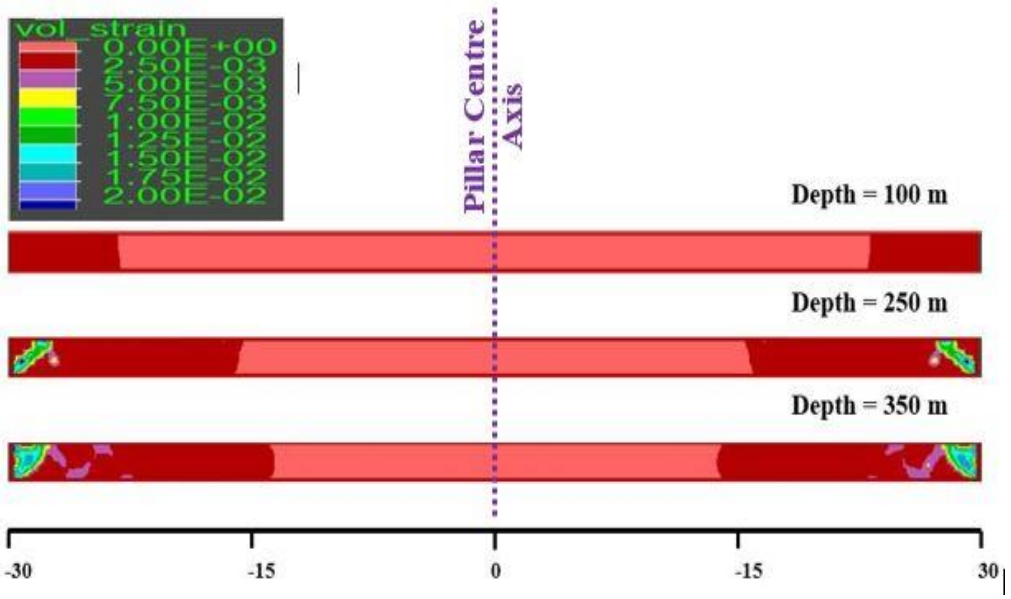

Figure 5.1. Volumetric strain across pillar width at a cover depth of 100, 250, and 350 m

The plot of the extent of positive volumetric strain zones (% ZoPVS) vs. cover depth (Figure 5.2) shows that the ZoPVS increases linearly with an increase in the cover depth. It represented the degrading condition of the pillar with the increase in cover depth. For the 60 m wide pillar, the ZoPVS was only 23.5 % for the cover depth of 100 m, which increased to 56.4 % for the increased cover depth of 350 m.

A parallel study was undertaken to assess the effect of cover depth on undersized pillars by reducing the pillar width from 60 m to 30 m. Figure 5.2 shows the comparative plot of ZoPVS

at the cover depth of 100-350 m. The study showed that extent of ZoPVS increased sharply for a reduced pillar size of 30 m compared to the nominal pillar of 60 m for the given range of cover depth. The ZoPVS was 43.8% at the cover depth of 100 m and occupied the entire pillar for the cover depth of 350 m.

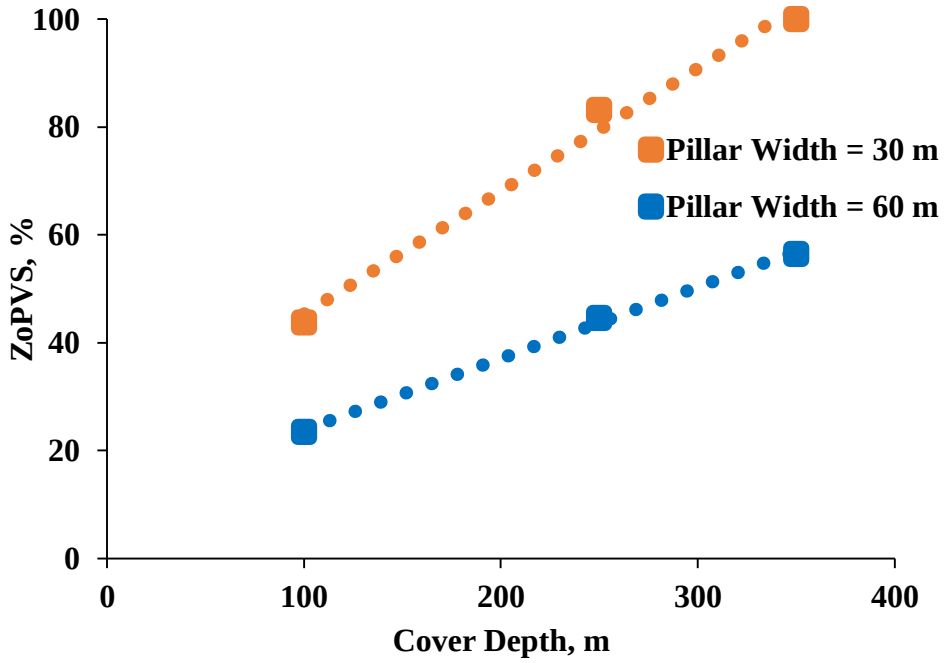

Figure 5.2. ZoPVS vs cover depth plot for pillar width of 30 m and 60 m

The PWBP of 60 m width subjected to a constant water head of 125 m showed an increasing trend of steady-state seepage rate with the cover depth (Figure 5.3). A seepage rate of 1.5×10^{-3} $m^3/s/km$ (23.8 GPM/km) was observed at a cover depth of 100 m, which increased to 1.6×10^{-3} $m^3/s/km$ (24.8 GPM/km) for a cover depth of 350 m. However, for the reduced pillar width of 30 m, the observed seepage rate at 100 m cover depth was 3×10^{-3} $m^3/s/km$ (47.7 GPM/km), which increased drastically to 6.6×10^{-3} $m^3/s/km$ (105.4 GPM/km) at a

cover depth of 350 m. The study confirmed a close relationship between the ZoPVS, representing the mechanical performance of the pillar, and the seepage rate signifying its hydraulic performance.

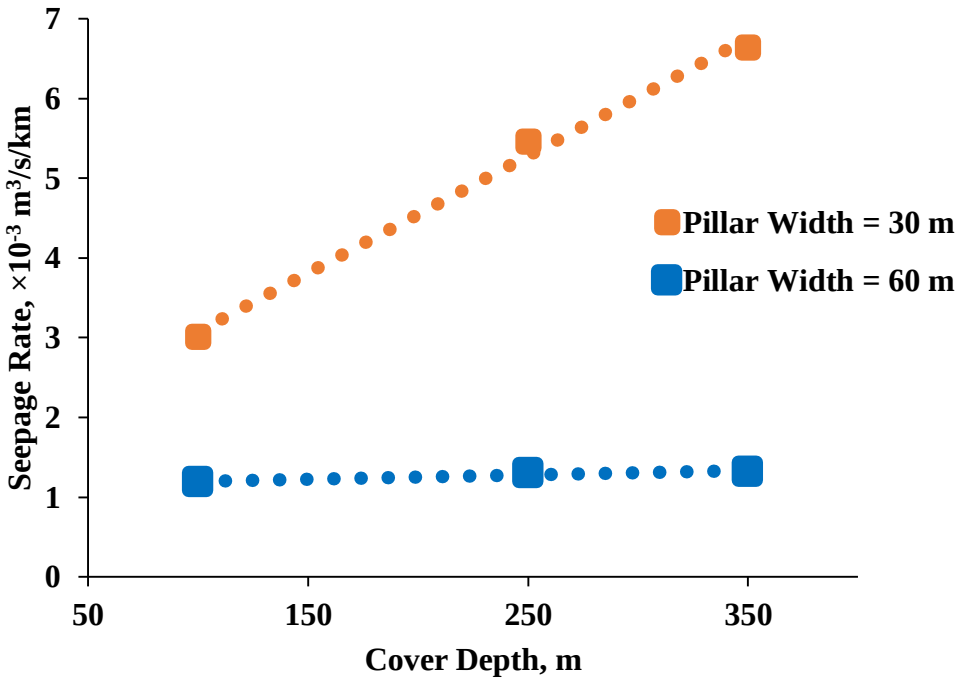

Figure 5.3. Seepage rate vs cover depth plot for a constant water head of 125 m for 30 m and 60 m wide barrier pillars

The study of field data suggested that the maximum water head can be equal to the cover depth. Hence, the seepage rate can be very high at a higher cover depth compared to the shallow depth working even for the same width of the PWBP. To validate this consideration, a separate study was conducted for PWBP of 30 and 60 m width considering water head of 50 % of cover depth. The water head was maintained at 50 % of the cover depth, which resulted in its variation from 50-175 m for cover depths of 100-350 m. The plot of seepage

rate vs. cover depth (Figure 5.4) showed that the seepage rate through PWBP increased following a similar trend with the cover depth. However, the slope of the plot indicated a sharper increase in the rate of water seepage as compared to the previous case (Figure 5.3) when the water head was constant. For a 60 m wide pillar, the seepage rate of 0.5×10^{-3} $m^3/s/km$ (7.6 GPM/km) was observed at a 100 m cover depth, which increased to 1.8×10^{-3} $m^3/s/km$ (29.2 GPM/km) at a cover depth of 350m. For a 30 m wide barrier pillar, the seepage rate of 1.2×10^{-3} $m^3/s/km$ (19.1 GPM/km) was observed at a cover depth of 100 m, which increased to 9.3×10^{-3} $m^3/s/km$ (147.6 GPM/km) at a cover depth of 350 m. The change in the seepage rate for the 30 m wide pillar was steeper than for the 60 m wide pillar.

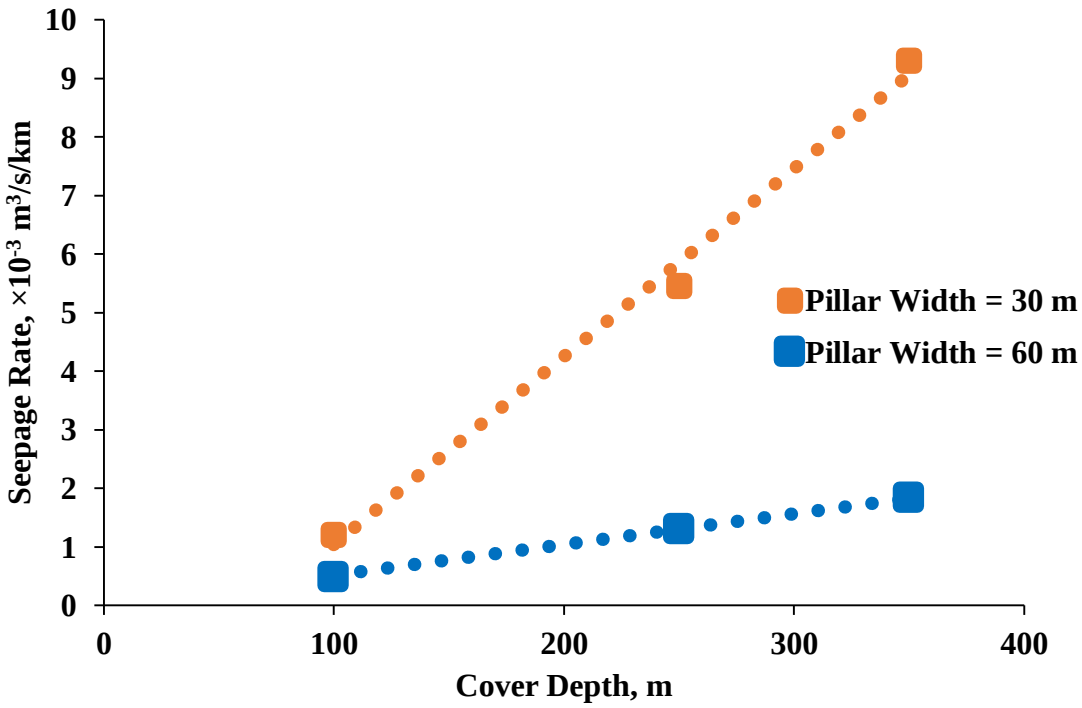

Figure 5.4. Seepage rate vs cover depth for water head of 50 % of cover depth for 30 m and 60 m wide barrier pillars

5.3 Effect of Pillar Width

The effect of pillar width on the volumetric strain and seepage rate characteristics of PWBP was studied for pillar widths of 30, 60, 90, and 120 m. The maximum width corresponds to twice the minimum width required per the regulatory provisions of CMR 2017.

The plot of volumetric strain (Figure 5.5) shows that the ZoPVS increased with the reduction in the pillar width. For the 120 m wide pillar, the ZoPVS was 23 %, and it increased to 100% for the 30 m width. The remaining zones having zero volumetric strain, formed the intact core of the pillar. This core, unaffected by the loading of the pillar, reduced with the width of the PWBP. The pillar showed an asymptotically increasing trend of ZoPVS for reducing pillar width from 120 m to 30 m (Figure 5.6).

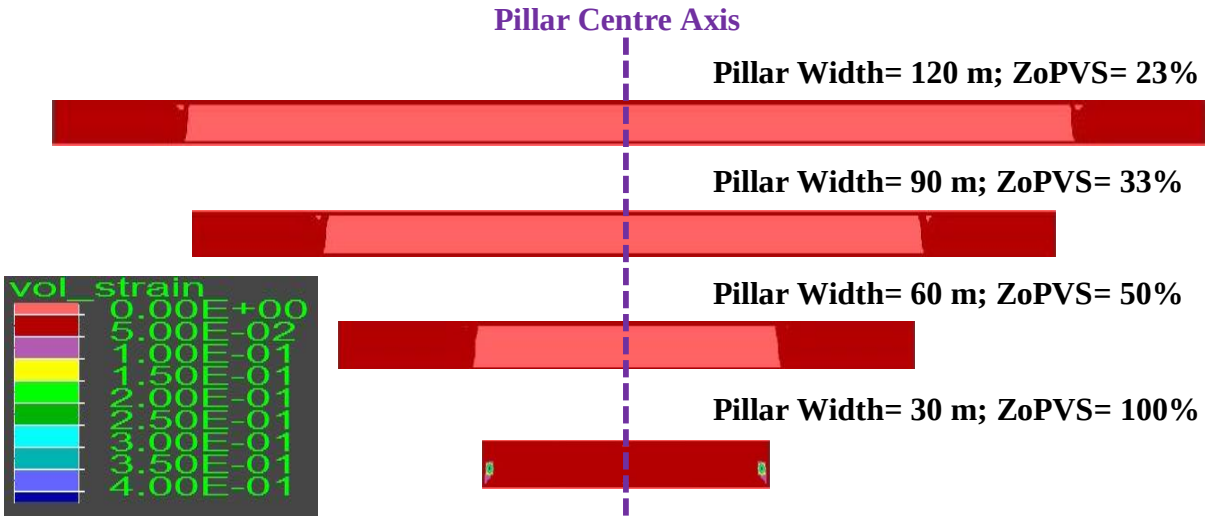

Figure 5.5. Volumetric strain across the pillar for 30, 60, 90, and 120 m wide PWBP

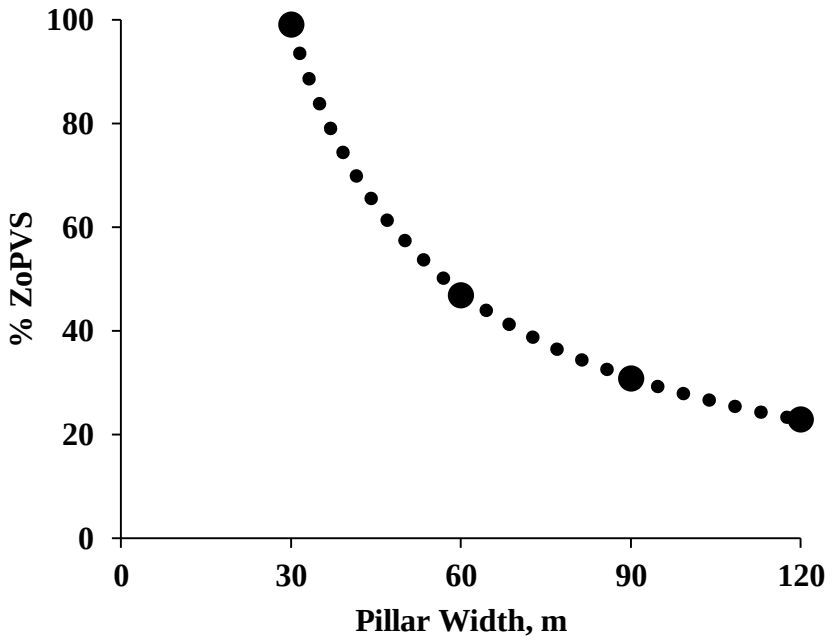

Figure 5.6. ZoPVS vs PWBP width

The plot of seepage rate vs. PWBP width (Figure 5.7) showed an increased water seepage rate with a reduction in the pillar width. The water seepage rate of 0.8×10^{-3} $m^3/s/km$ (12 GPM/km) was observed for the 120 m wide pillar, which grew to 5.5×10^{-3} $m^3/s/km$ (86.58 GPM/km) for the 30 m wide pillar. The asymptotic trend for change in seepage rate (Figure 5.7) is similar to the ZoPVS (Figure 5.6) trend w.r.t. PWBP width. The ZoPVS induced in the 30m wide pillar was 100 %, which resulted in a sharp increase in the seepage rate through the pillar as the zones with positive volumetric strain failed to provide hydraulic resistance, indicating its unstable behaviour for piping failure. The rate of change in seepage rate reduced as the extent of ZOPVS reduced with the increase in the pillar width and became almost flat beyond a certain pillar width.

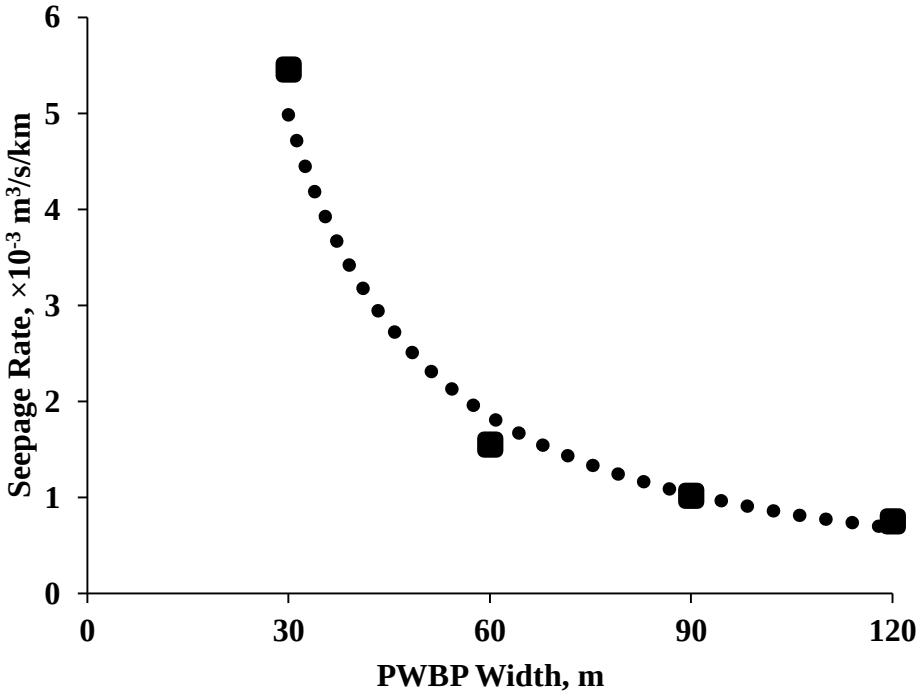

Figure 5.7. Seepage rate vs PWBP width

5.4 Effect of In-situ Permeability

The site-specific data on permeability for Indian coal seams are not readily available, and the accompanying uncertainty of various measurement methods is also significant. The permeability can range from 0.01 to 100 mD (9.9×10^{-15} to 9.9×10^{-11} m^2/Pa.sec.) in undisturbed coal to much higher values in stressed pillars as per the data compiled in Table 2.5. Accordingly, the parametric study has been carried out for in-situ permeability of 0.3, 25, and 100 mD.

The seepage rate vs. permeability plot (Figure 5.8) shows that the seepage rate increased linearly with the permeability. The seepage rate of 0.02×10^{-3} m^3/s/km (0.3 GPM/km) was observed for the permeability of 0.3 mD, which increases to 6.2×10^{-3} m^3/s/km (98.3 GPM/km) for 100 mD. Although the state of stress-dependent volumetric strain induced

across the pillar remained the same, the corresponding induced permeability was high for the high in-situ permeability of the rock. Therefore, higher seepage rate was observed through a pillar having higher in-situ permeability.

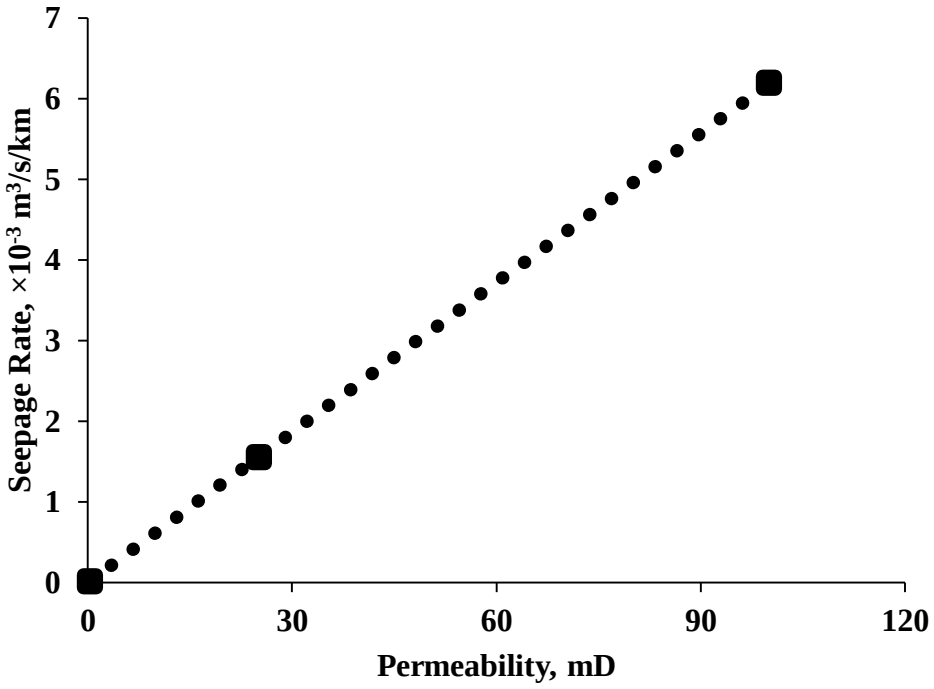

Figure 5.8. Seepage rate vs permeability

Figure 5.9(a, b) depicts the profile of induced vertical and horizontal stresses in 30 to 120 m wide barrier pillars formed of soft coal at the cover depth of 350 m. The peak vertical and horizontal stresses increased with the decrease in pillar width. The extent of the intact zone decreased from 70 % to almost zero, while the yield zone increased from 39 to 97 %. For the critical width of 30 m with no intact zone remaining in the pillar, the extent of induced positive volumetric strain zones increased sharply, causing the pillar to become unstable

(Figure 5.9c). This was also characterised by a sharp change in induced permeability in the yield zone having positive volumetric strain (Figure 5.9d).

The induced vertical stress was limited to 20-27 MPa for the pillar width of 120-60 m. The stress in the core was lower w.r.t. the edges in these cases. However, as the pillar width was reduced to 30 m, the peak-induced stress shifted from the edges, and the core received the maximum stress of 45 MPa at the cover depth of 350 m, which is 5.14 times the in-situ vertical stress.

The edges of the pillar were almost distressed irrespective of the pillar size, while the core held a higher confining stress of 10-18 MPa. The peak confining stress increased to 18 MPa for the pillar width of 30 m. However, the width of the core zone reduced with the reduction in pillar width.

The plot of induced permeability (Figure 5.9 c) and ZoPVS also confirmed these trends. For pillar width higher than its critical value, the induced permeability was higher at the edges, and the pillar had a significant core in intact condition. However, the induced permeability increased significantly, covering the whole pillar and the intact zone in the pillar was left to a negligible value with the reduction in pillar width to its critical limit.

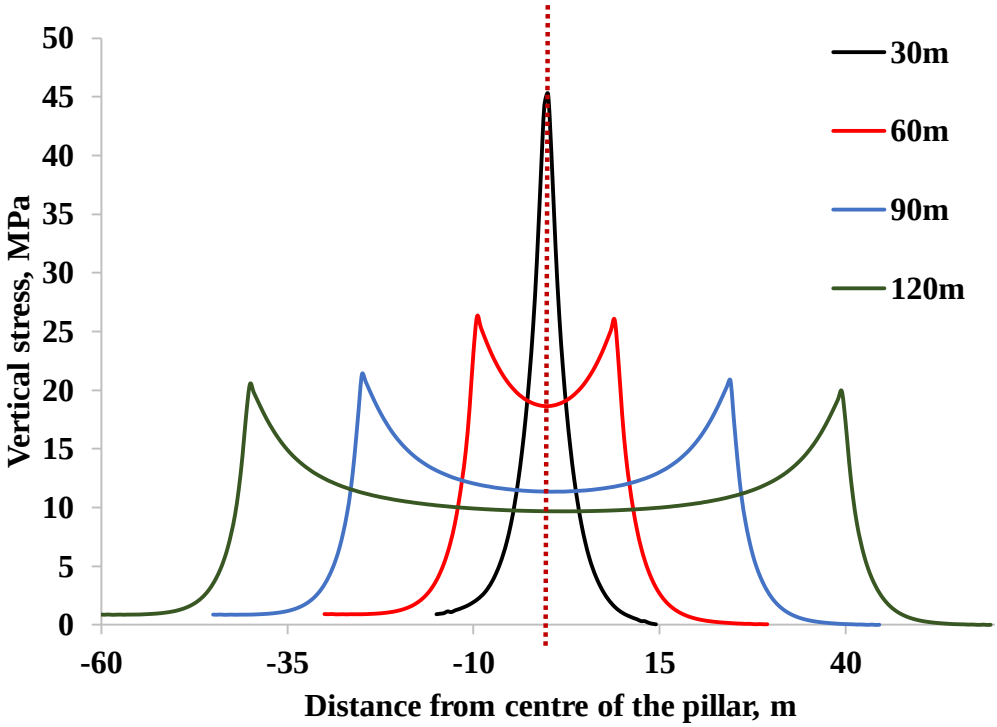
Vertical stress, MPa
50
45
40
35
30
25
20
15
10
5
0
-60
-35
-10
15
40
Distance from centre of the pillar, m
30m
60m
90m
120m

(a)

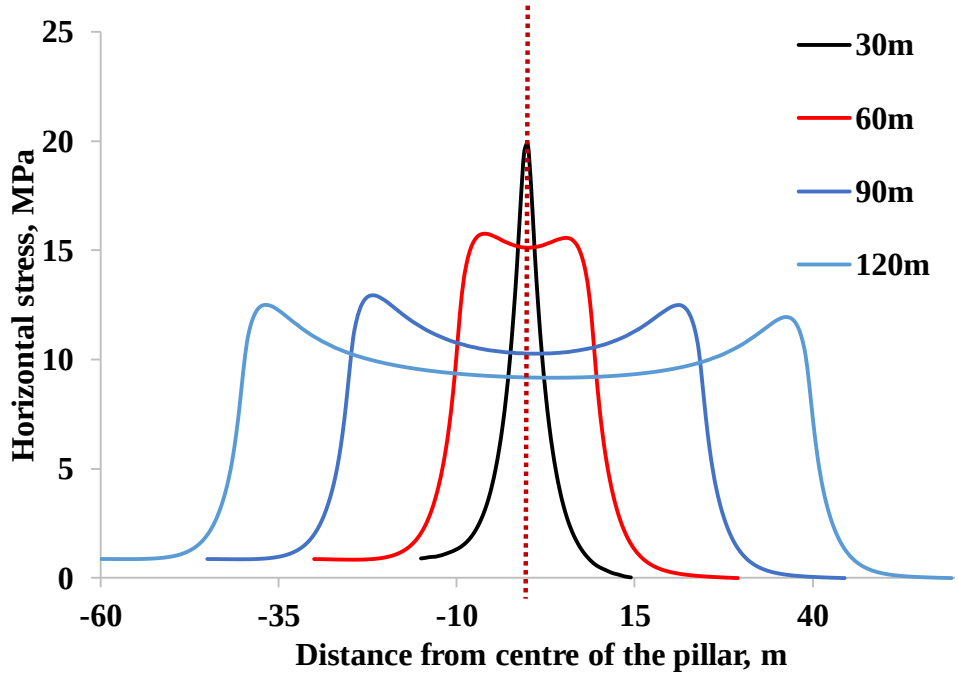
Horizontal stress, MPa
25
20
15
10
5
0
-60
-35
-10
15
40
Distance from centre of the pillar, m
30m
60m
90m
120m

(b)

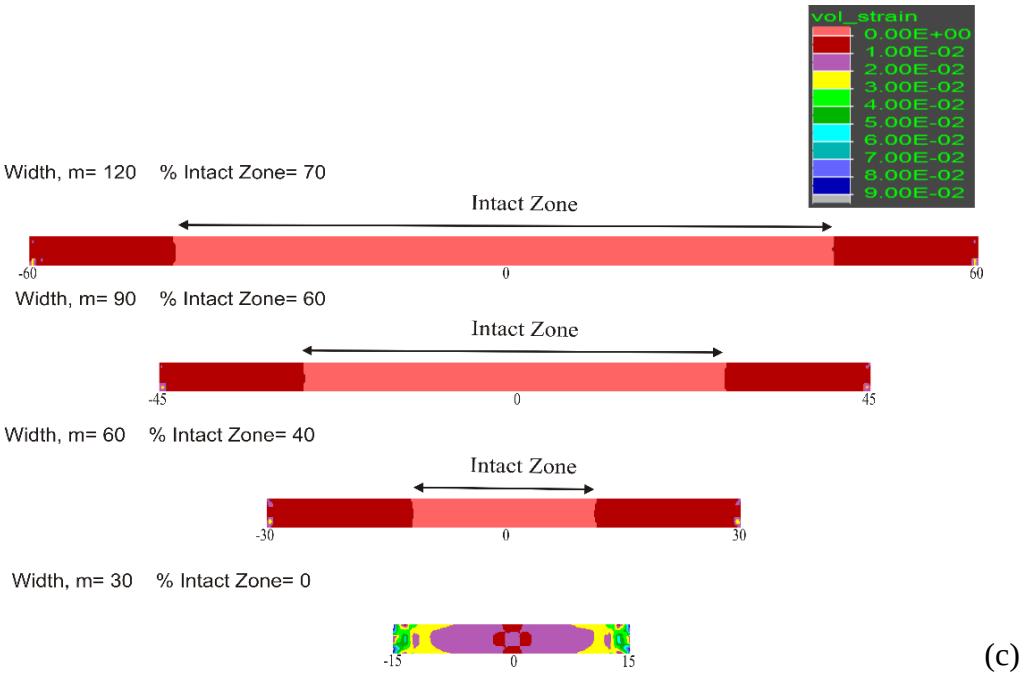

(c)

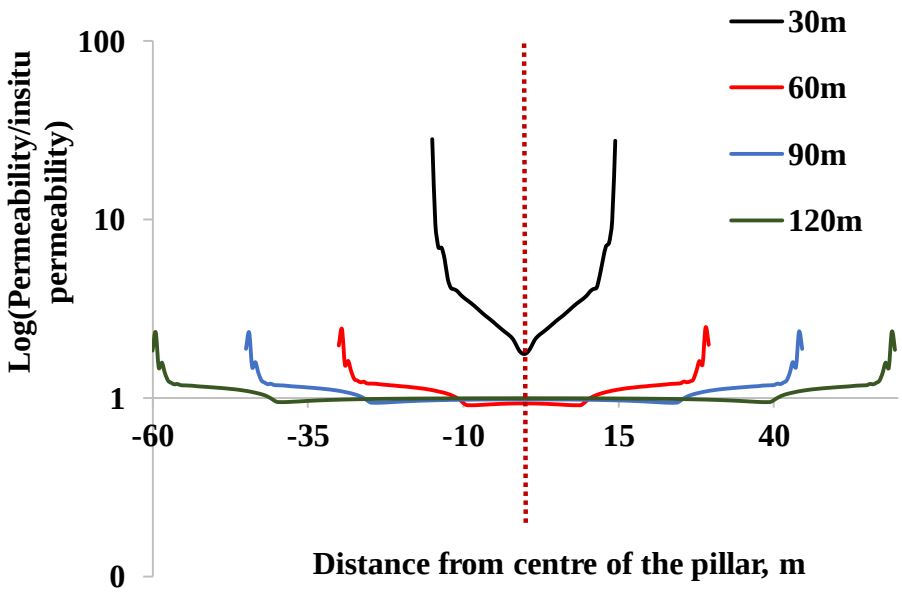

(d)

Figure 5.9. (a) Average vertical stresses (b) Average horizontal stresses (c) Induced permeability, and (d) Volumetric strain contour across different widths of barrier pillar of 3 m height and soft coal at a depth of 350 m

5.5 Effect of Water Head

The parametric study for the water head was conducted for 62.5 m (25% of cover depth), 125 m (50% of cover depth), and 250 m (100% of cover depth) for the pillar width of 60 m.

The plot of seepage rate vs. water head (Figure 5.10) shows that the seepage rate followed a linearly increasing trend with the increase in the water head from 62.5 to 250 m (25–100% of cover depth) and moderate permeability and strength of rock. The seepage rate of 0.8×10^{-3} $m^3/s/km$ (12.3 GPM/km) was observed for 62.5 m of water head, which increased to 3.1×10^{-3} $m^3/s/km$ (49.3 GPM/km) for water head of 250 m. The observed change in the seepage rate w.r.t. the water head was directly proportional, as the four-fold increase in a water head from 62.5 m to 250 m increased the seepage rate by four times to 3.1×10^{-3} $m^3/s/km$ (49.3 GPM/km).

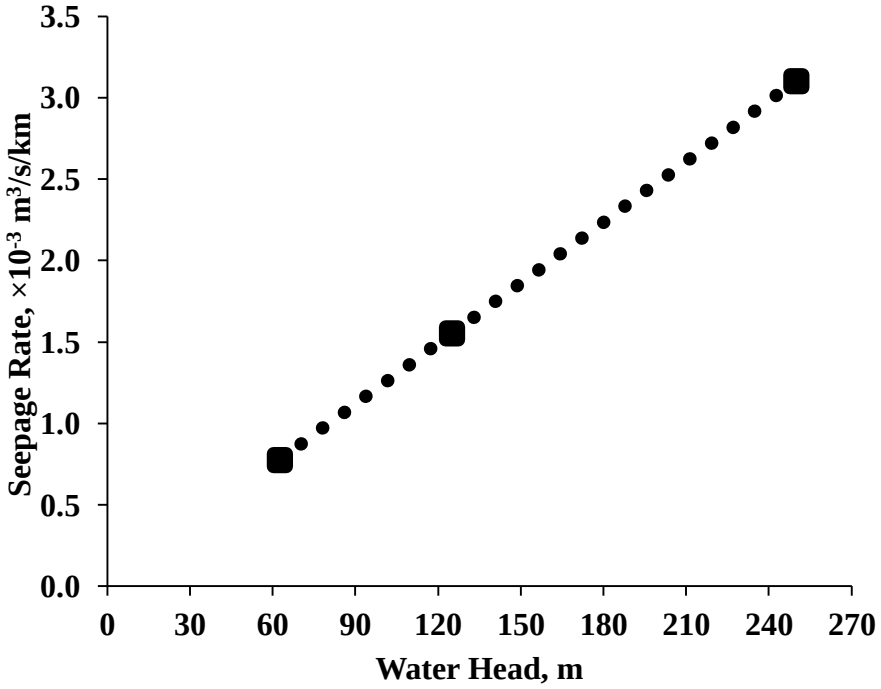

Figure 5.10. Seepage rate vs water head

5.6 Effect of Rockmass Strength

The strength properties of coal and nether roof and floor were classified into three categories: soft, average, and hard, based on the conditions prevailing in different coalfields in India (Singh, 2007). The corresponding data for the rock mass are given in Table 5.3.

Table 5.3 Rock mass strength properties used in FLAC 2D modelling

Rock Type	Density, Kg/m^3			Elastic Modulus, GPa			UCS, MPa			Tensile strength, MPa		
	hard	average	soft	hard	average	soft	hard	average	soft	hard	average	soft
Roof, floor	2373	2212	1879	13.37	8.50	3.01	20.92	11.68	4.01	2.39	1.22	0.39
Coal	1440	1392	1240	2.00	2.00	2.00	6.32	3.87	2.04	0.71	0.35	0.04

The study showed that the seepage rate increased linearly as the rock mass strength decreased from hard to soft (Figure 5.11). The seepage rate for low strength was 1.6×10^{-3} m^3/s/km (25.8 GPM/km), which was reduced to 1.5×10^{-3} m^3/s/km (23.6 GPM/km) for the hard rock. The model did not indicate a significant change in the rate of seepage for a given pillar width with the change in the strength of the rock material. An in-depth scrutiny of the data revealed that the strength ratio σ_c/σ_t varied from 8–10 for the hard and soft conditions of the rock. The long-term water flow through the pillar was expected to modify the permeability and porosity characteristics of the rock as a function of positive volumetric strain, as hypothesised in this study. With reducing resistance and increasing rate of water flow till achievement of the steady state condition, the rock mass of the pillar was expected to absorb a significant amount of water, causing a drastic reduction in its effective strength irrespective of its initial strength.

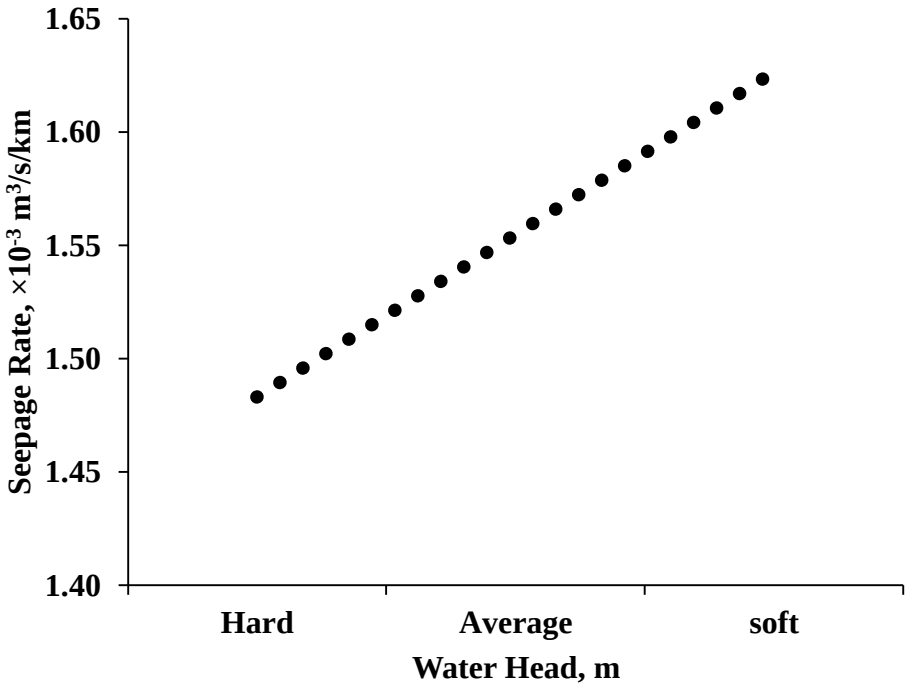

Figure 5.11. Seepage rate vs rock mass strength

5.7 Effect of Flow Regimes

Figure 5.12 shows the results of the parametric study incorporating variations in the flow regime as flow through pillar only, roof only, floor only, pillar and roof, pillar and floor, and the pillar system (roof- pillar-floor).

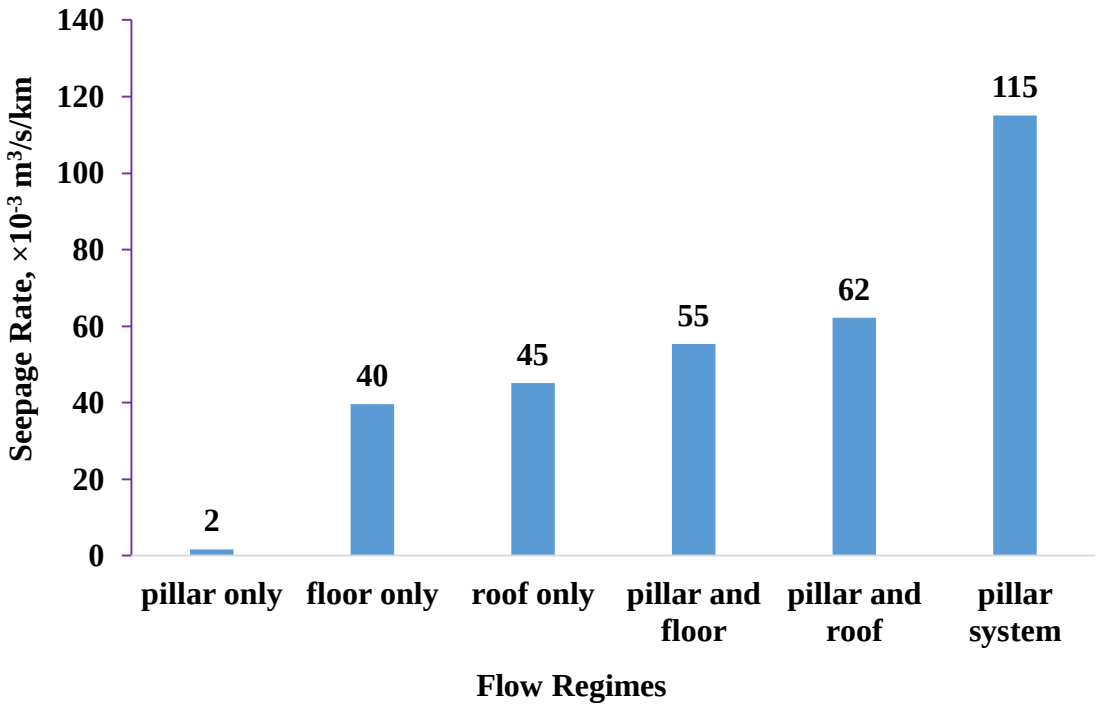

Figure 5.12. Seepage rate for different flow regimes

The seepage rate across the barrier pillar increased as the roof and/or floor participated in the flow. The immediate roof and floor are generally composed of sandstone which is highly permeable as compared to the pillar, which is formed of coal (almost an impermeable material). The model observed seepage rate through the pillar only was 2×10^{-3} m^3/s/km (24.6 GPM/km) while it was 40×10^{-3} m^3/s/km (629.2 GPM/km) through the floor and 45×10^{-3} m^3/s/km (715.7 GPM/km) through the roof only condition. The seepage rate through the roof was high compared to the floor, as it was supported by gravity. Similarly, the observed seepage rate for pillar and floor combined and pillar and roof combined were 55×10^{-3} m^3/s/km (877.8 GPM/km) and 62×10^{-3} m^3/s/km (986.0 GPM/km), respectively. The combined seepage rate observed through pillar, roof and floor was not just an algebraic sum of seepage rate through pillar only, roof only, and floor only. The seepage rate through

the pillar system (roof, pillar, and floor combined) was 115×10^{-3} $m^3/s/km$ (1827.0 GPM/km).

5.8 Summary

A numerical modelling study was carried out to assess the hydro-mechanical behaviour of PWBP under different geo-mining conditions. The parametric study showed that irrespective of material strength, the PWBP in permeable rock mass in deep mining conditions may lead to hydro-mechanical instability, which can be avoided by its careful design.

An increase in cover depth can lead to the transfer of a higher load on a pillar for a given extraction percentage. Under-designed Barrier pillars may develop a significantly larger extent of ZoPVS under such a condition, which is prone to mechanical and hydraulic failure when subject to a water head in the worst conditions. The decreased width of intact zones in the pillar reduced the effectiveness of the pillar, allowing a high water seepage rate. The higher permeability of rock mass worsened the situation further by facilitating the seepage rate of water. Higher rock mass strength provided only marginal support to the stability of the PWBP as the weakening caused by the water absorption reduced its effective strength drastically in the water-saturated condition. The pillar system produced the worst rate of water seepage among the possible flow regimes.